Journal of Sound and Vibration ▮ (▮▮▮▮) ▮▮▮–▮▮▮

Contents lists available at ScienceDirect

Journal of Sound and Vibration

journal homepage: www.elsevier.com/locate/jsvi

A torsion quasi-zero stiffness vibration isolator

Jiaxi Zhou [a], Daolin Xu [a,*], Steven Bishop [b]

[a] State Key Laboratory of Advanced Design and Manufacturing for Vehicle Body, College of Mechanical and Vehicle Engineering, Hunan University, Changsha 410082, PR China

[b] Department of Mathematics, University College London, Gower Street, London WC1E 6BT, UK

ARTICLE INFO

Article history:
Received 10 July 2014
Received in revised form
30 September 2014
Accepted 17 October 2014
Handling Editor: D.J Wagg

ABSTRACT

A torsion vibration isolator with quasi-zero stiffness (QZS) is proposed to attenuate the transmission of torsional vibration along a shaft system, which also plays a role of coupling between shafts. A pre-compressed cam–roller mechanism is designed to provide torsional negative stiffness that counteracts with the positive torsion stiffness of the vulcanized rubber between shafts. With the design parameters are set to satisfy a unique condition, the stiffness of the isolator delivers a QZS property about the equilibrium position. A nonlinear mathematical model is developed and its dynamic characteristics are further analyzed by using the Harmonic Balance method. A typical folded resonance curve occurs when the vibration amplitude is plotted as the excitation frequency is varied, illustrating a jump phenomenon in the response. The efficiency of vibration attenuation is estimated under a designed torque load, showing that the torsion QZS vibration isolator outperforms the corresponding linear counterpart, especial in low frequency ranges. Furthermore, the torque transmissibility of the QZS isolator is also studied to demonstrate the performance of the QZS isolator when the actual torque deviates from the design load.

1. Introduction

Generally, a passive linear isolator, such as coil spring or rubber mount, can attenuate vibration only when excitation frequencies are larger than $\sqrt{2}$ times of the natural frequency of the isolation system. Thus, an isolator with small stiffness is usually desired to extend the effective band-width of isolation to improve the isolation performance, but it will also result in large deflection, leading, in some sense, to instability. Ideally, a passive vibration isolator should possess high static stiffness and low dynamic stiffness, not only to firmly support a large weight mass but also to effectively isolate vibration over a large band-width. Fortunately, a type of isolator combining positive stiffness and negative stiffness elements has been proposed to fulfill supercritical vibration isolation performance. By balancing the positive stiffness and the negative stiffness at an equilibrium position under a designed loading weight, it leads to the property of high static stiffness and low dynamic stiffness, so-called quasi-zero-stiffness isolator.

Quasi-zero-stiffness (QZS) isolators have been studied in depth over the last two decades; here we offer a brief review. Investigations on design concepts and dynamic characteristics of the QZS isolator have been well documented. Carrella et al. [1,2] constructed a simple model of QZS isolator by connecting, in parallel, a vertical spring with oblique springs, and studied its static and dynamic characteristics of the QZS isolator. Theoretical analysis indicated that the QZS isolator outperforms the

* Corresponding author.
E-mail addresses: jxizhou@hnu.edu.cn (J. Zhou), dlxu@hnu.edu.cn (D. Xu).

http://dx.doi.org/10.1016/j.jsv.2014.10.027
0022-460X/

Please cite this article as: J. Zhou, et al., A torsion quasi-zero stiffness vibration isolator, *Journal of Sound and Vibration* (2014), http://dx.doi.org/10.1016/j.jsv.2014.10.027

corresponding linear one under excitations whose amplitude is smaller than some critical value. Nonlinear dynamic behaviors of this kind of QZS vibration isolation system, such as the occurrence of period-doubling bifurcation and its development into chaos motion, were reported by Kovacic et al. [4]. In our previous work [5], prototypes of QZS isolators were built by connecting a vertical coil spring with four oblique coil springs. And then experiment tests were carried out to verify the benefits of the QZS isolator, especially for low-frequency excitations. Using specific planar springs instead of coil springs, Lan et al. [6] developed a QZS isolator and carried out the experimental test, and emphatically studied the effect of applied loads on isolation performances. For a potential application in attenuating vibration of the vehicle seat, Le and Ahn [7] studied the displacement transmissibility of the QZS isolator consisting of coil springs, and results showed that adding negative stiffness mechanism notably improves the isolation performance.

In addition to the oblique springs, the negative stiffness mechanism can be realized by other ways. Platus [8] proposed a compact QZS isolator using a laterally loading flexural beam as the negative stiffness element to cancel the stiffness of the spring suspension, and thereby producing ultra-low resonant frequency of the vibration isolation system. Yang et al. [9] studied dynamic and power flow behaviors of this type of QZS isolator, and it was also found that adding negative stiffness mechanism can greatly enlarge the frequency band for effective vibration isolation. Carrella and Friswell [10] developed a QZS isolator by connecting a coil spring in parallel with a composite bistable plate. Further, Shaw et al. [11] built an apparatus of this type of QZS isolator, and tested the vibration isolation performance under base excitations, which shows a greater isolation region and a lower peak response than the equivalent linear system. Sun et al. [12] proposed an isolation platform with *n*-layer scissor-like truss structure to achieve QZS property. Carrella et al. [3] developed a QZS isolator by combining coil springs and magnets arranged by attracting configuration to act as negative stiffness element. Robertson et al. [13] presented a QZS isolator by using a magnetic levitation system. Xu et al. [14] proposed a QZS isolator consisting of horizontal magnetic springs and vertical coil spring for verifying the performance of low-frequency band isolation. Wu et al. [15] also developed a magnetic spring with negative stiffness to counteract the positive stiffness of the system to pursue excellent isolation performance.

Additionally, active control combined into the QZS system is beneficial to dealing with the situation of altering applied loads, and to further improving isolation performance. Zhou and Liu [16] devised a tunable electromagnetic isolator with high-static–low-dynamic stiffness to obtain a low and near constant dynamic stiffness by controlling the gap distance and the current. Sun et al. [17] utilized a time-delay active controller to improve both the robustness and the transmissibility performance of the QZS vibration isolation system.

There are a number of design concepts for constructing negative stiffness mechanisms or structures; interesting readers can refer to the monograph by Alabuzhev et al. [18] and the comprehensive review report by Ibrahim [19]. However, almost all the QZS isolators to date have only focused on translational vibration attenuation. To the best knowledge of authors, none has reported QZS isolators for attenuating torsional vibration.

In this paper, a novel QZS isolator for torsion vibrations is proposed, which is installed in between two segments of shafts, to reduce torsional vibration along shaft. The two segments of shafts are coupled by vulcanized rubber that provides positive stiffness. A *cam–roller* mechanism is attached to the two segments of shafts to offer the negative stiffness. Carefully designing the rubber stiffness and *cam–roller* mechanism to satisfy a unique relationship of zero-stiffness condition, the torsion stiffness of the isolator becomes zero at the equilibrium position of the loaded isolator.

The study covers the static and dynamic characteristics of this QZS torsional vibration isolator. The expression of the restoring torque is deduced by static analysis, which is approximated by a polynomial function using a Taylor series expansion up to the order of 7, in order to precisely analyze the dynamic behaviors of the vibration isolation system. The nonlinear equation of motion of the QZS model is solved analytically by using the Harmonic Balance method, which determines the relationship between the torsion angle amplitude and excitation frequency. Furthermore, the theoretical ranges of excitation amplitude and damping factor are restricted under the condition that cam and roller must remain in contact. The vibration isolation performance of the torsion QZS isolator is evaluated using torque transmissibility, which is also compared with the corresponding linear isolator that only contains the positive stiffness element of the QZS isolator. The paper is organized as follows. Section 2 gives the QZS model and static characteristics. In Section 3, the nonlinear dynamic model is developed, and the amplitude–frequency relationship is obtained analytically. The dynamic behavior and vibration isolation performance are shown in Section 4. The influence of actual transmission torque deviating from the designed torque on the isolation performance is discussed in Section 5. Finally, Section 6 draws some conclusions of this work.

2. Statement of the model and static analysis

Fig. 1 shows a schematic diagram of the proposed QZS torsional vibration isolator at the static equilibrium position. The two ends of the isolator are connected with shafts, not only to transmit a designed torque but also to isolate the torque oscillation of one shaft from the other. The right shaft connector (7) is elastically connected with the left shaft connector (6) through vulcanized rubber (5), which forms a traditional shaft coupling. The rubber also plays a role of linear vibration isolator, which provides a positive torsion stiffness k_θ (N · m/rad). Four cylindrical cams (1) are symmetrically distributed on the left shaft connector (6), and contact with four rollers (2) mounted on right shaft connector (7), respectively. Note that the number of the cylindrical cam is not limited to be four, and it can be selected as N ($N \geq 2$) depending on the geometrical dimensions of the parts and the design requirement. In this paper, we take $N=4$ as an example. Roller (2) is held by

Please cite this article as: J. Zhou, et al., A torsion quasi-zero stiffness vibration isolator, *Journal of Sound and Vibration* (2014), http://dx.doi.org/10.1016/j.jsv.2014.10.027

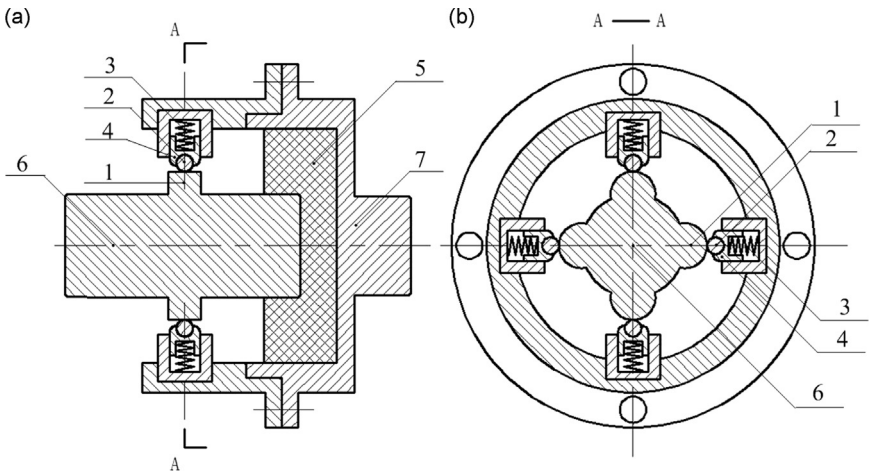

Fig. 1. Schematic diagram of the QZS torsional vibration isolator. (a) longitudinal-sectional view of assembly (b) cross-sectional view. Labels: 1-cam with radius r_2, 2-roller with radius r_1, 3-spring, 4-slider, 5-vulcanized rubber cam, 5 cylinder roller, 6-left shaft connector, 7-right shaft connector.

slider (4), so that can only move in the radial direction of the shafts and the slider is supported by a spring (3) that has a stiffness of k_h (N/m), as shown in Fig. 1b. The friction between the cylindrical cam (1) and the roller (2) is neglected because of rolling contact. There are four pairs of cylindrical cam and roller in this model, which are purposely designed to provide negative torsional stiffness to the isolator. When the negative stiffness of the cam and roller pairs and the positive stiffness of rubber reach a balance at equilibrium position, the isolator will possess the QZS property. At the static equilibrium position, the centers of a pair of the cylindrical cam and roller align with the center of the shafts, as shown in Fig. 1b, and the static torsional angle of the left shaft relative to the right one is $\theta_0 = M_0/k_\theta$, and the compressed deflection of the spring (3) is denoted as δ.

When the system is at rest, namely no loading torque applied on the isolator, as shown in Fig. 2a, the positive torsion stiffness will cause a rotational offset $\theta = -\theta_0$ from the static equilibrium position (Figs. 1b and 2b). It should be noted that the sign of torsion angle is designated to be positive when the left shaft connector (6) with cams clockwise turns relative to the right one. As the system starts turning and the load slowly increases, the angle θ will increase until $\theta=0$ when the applied torque load is equal to the design torque M_0, and the isolator reaches its static equilibrium state, as shown in Figs. 1b and 2b.

As the torque on the shaft increases from M_0 by M to $M_1=M_0+M$, there is a torsional deformation of the QZS isolator, i.e. a rotational displacement θ of the left shaft connector relative to the right hand shaft, as shown in Fig. 2c. The static equilibrium equation of the shaft connector with the cams can be given by

$$M_1 = M_0 + M = M_2 - 4Fd \tag{1}$$

where $M_2 = k_\theta(\theta_0+\theta)$ is the restoring torque of the rubber, and F is the contact force between a pair of the cam and roller, and d is the orthogonal distance between the force vector F and the center of the shaft. According to the geometric relationship and static balance condition, F and d are given by

$$F = \frac{k_h[\delta-(r_1+r_2+r_3)+z_1](r_1+r_2)}{z_1 - r_3\ \cos\ \theta}, \quad d = \frac{z_1 r_3\ \sin\ \theta}{r_1+r_2} \tag{2}$$

where

$$z_1 = r_3\ \cos\ \theta + \sqrt{(r_1+r_2)^2 - r_3^2 \sin^2\theta} \tag{3}$$

Recalling that $M_0 = k_\theta\theta_0$ and substituting the expressions for M_2, F, and d into Eq. (1), the incremental torque M related to the torsion angle θ can be determined by

$$M = k_\theta\theta - 4\frac{k_h[\delta-(r_1+r_2+r_3)+z_1]z_1 r_3\ \sin\ \theta}{z_1 - r_3\ \cos\ \theta} \tag{4}$$

It should be noted that we only consider small torsional oscillations in our analysis. The cylindrical cam and roller pair is assumed to always remain in contact in the above analysis for the static force. The disengagement between a pair of the cylindrical cams and rollers could occur under large excitations, but we consider this to be out of the scope of the present work. Therefore, the expression of the torque M in Eq. (4) is valid for a range of angular displacement $|\theta| \le \theta_c$, which is defined by

$$\theta_c = \arccos\frac{(r_1+r_3)^2 + r_3^2 - (r_1+r_2)^2}{2r_3(r_1+r_3)} \tag{5}$$

Please cite this article as: J. Zhou, et al., A torsion quasi-zero stiffness vibration isolator, *Journal of Sound and Vibration* (2014), http://dx.doi.org/10.1016/j.jsv.2014.10.027

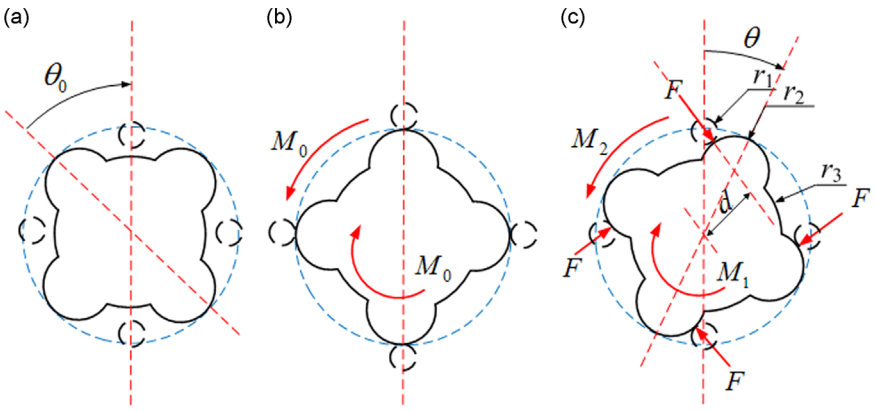

Fig. 2. Schematic diagram of static analysis of the shaft connector with cams. (a) rest position; (b) static equilibrium position; (c) torsion angle θ from static equilibrium position resulting from a incremental torque M to M_0.

The stiffness of the isolator can be obtained by differentiating the torque M with respect to the torsion angle θ, given as

$$k=\frac{\mathrm{d}M}{\mathrm{d}\theta}=k_\theta-4k_h\frac{z_2-z_3}{(z_1-r_3\ \cos\ \theta)^2} \tag{6}$$

where

$$z_2=\left\{\frac{\mathrm{d}z_1}{\mathrm{d}\theta}r_3z_1\ \sin\ \theta+[\delta-(r_1+r_2+r_3)+z_1]r_3\left(z_1\ \cos\ \theta+\frac{\mathrm{d}z_1}{\mathrm{d}\theta}\ \sin\ \theta\right)\right\}(z_1-r_3\ \cos\ \theta)$$
$$z_3=[\delta-(r_1+r_2+r_3)+z_1]r_3z_1\ \sin\ \theta\left(\frac{\mathrm{d}z_1}{\mathrm{d}\theta}+r_3\ \sin\ \theta\right) \tag{7}$$

There is a unique condition among the parameters of k_θ, k_h, r_1, r_2, r_3 and δ, which results in the zero stiffness characteristic at the equilibrium position. This condition is achieved by setting $k(\theta=0)=0$, given as

$$\frac{k_\theta}{k_h(r_1+r_2)^2}=4\bar{r}_3(1+\bar{r}_3)\bar{\delta} \tag{8}$$

where $\bar{r}_3=r_3/(r_1+r_2)$, $\bar{\delta}=\delta/(r_1+r_2)$. Eq. (8) implies that the realization of the QZS property requires the stiffness of two elastic elements have to satisfy a relationship of the radius of the cam and roller as well as the initial compressed displacement of the spring. Furthermore, using the non-dimensional terms $\bar{M}=M/(k_\theta\cdot 1)$ and $\bar{z}_1=z_1/(r_1+r_2)$, and substituting Eq. (8) into Eq. (4), the relationship between the incremental torque and torsion angle can be written in a non-dimensional form as

$$\bar{M}_{\mathrm{QZS}}=\theta-\frac{1}{\bar{r}_3(1+\bar{r}_3)\bar{\delta}}\frac{\left[\bar{\delta}-(1+\bar{r}_3)+\bar{z}_1\right]\bar{r}_3\bar{z}_1\ \sin\ \theta}{\bar{z}_1-\bar{r}_3\ \cos\ \theta} \tag{9}$$

Note that the number '1' in the expression of $\bar{M}$ signifies 1 rad. Then, the non-dimensional stiffness can be written by

$$\bar{k}_{\mathrm{QZS}}=1-\frac{1}{\bar{r}_3(1+\bar{r}_3)\bar{\delta}}\frac{\bar{z}_2-\bar{z}_3}{(\bar{z}_1-\bar{r}_3\ \cos\ \theta)^2} \tag{10}$$

where $\bar{k}=k/k_\theta$, $\bar{z}_2=z_2/(r_1+r_2)^4$, $\bar{z}_3=z_3/(r_1+r_2)^4$.

In addition, if the number of the cam is selected to be N ($N\geq 2$), utilizing the above static analysis procedure, the incremental torque M related to the torsion angle θ can be given by

$$M=k_\theta\theta-N\frac{k_h[\delta-(r_1+r_2+r_3)+z_1]z_1r_3\ \sin\ \theta}{z_1-r_3\ \cos\ \theta} \tag{11}$$

and then, the stiffness can be given by

$$k=\frac{\mathrm{d}M}{\mathrm{d}\theta}=k_\theta-Nk_h\frac{z_2-z_3}{(z_1-r_3\ \cos\ \theta)^2} \tag{12}$$

By setting $k(\theta=0)=0$, the condition for QZS property is given by

$$\frac{k_\theta}{k_h(r_1+r_2)^2}=N\bar{r}_3(1+\bar{r}_3)\bar{\delta} \tag{13}$$

By substituting Eq. (13) into Eq. (11) and using the non-dimensional terms $\bar{M}=M/(k_\theta\cdot 1)$, $\bar{z}_1=z_1/(r_1+r_2)$, for the QZS isolator, the relationship between the incremental torque $\bar{M}_{\mathrm{QZS}}$ and torsion angle θ can be obtained, and it is found to be

Please cite this article as: J. Zhou, et al., A torsion quasi-zero stiffness vibration isolator, *Journal of Sound and Vibration* (2014), http://dx.doi.org/10.1016/j.jsv.2014.10.027

identical to Eq. (9) obtained in the case of $N=4$. Therefore, the selecting umber of the cam just has impact on the condition for QZS property, but has no influence on the torque–angle relationship.

It should be emphasized that $\overline{M}_{QZS}$ is an incremental torque to $\overline{M}_0$, and θ is the torsional angle deviating from the static equilibrium position. The torque–angle relationship from the rest position can be easily deduced from Eq. (9) by Coordinate translation. Let $\theta_1=\theta+\theta_0$ denote the torsional angle from the rest position, and $\overline{M}_{1,QZS}=\overline{M}_{QZS}+\overline{M}_0$ represent the applied torque. Obviously, at the rest position, $\theta_1=0$ and $\overline{M}_{1,QZS}=0$, namely $\theta=-\theta_0$ and $\overline{M}_{QZS}=-\overline{M}_0$. And at the equilibrium position, $\theta_1=\theta_0$ and $\overline{M}_{1,QZS}=\overline{M}_0$, namely $\theta=0$ and $\overline{M}_{QZS}=0$. That is, the torque applied on the isolator is $\overline{M}_0$ rather than 0 at the equilibrium position.

The static torsional angle θ_0 can be obtained by solving the equation of $\overline{M}_{QZS}(\theta=-\theta_0)=-\overline{M}_0$, given by

$$\theta_0=\arccos\frac{1-\bar{r}_3^2-\left[\bar{\delta}-(1+\bar{r}_3)\right]^2}{2\left[\bar{\delta}-(1+\bar{r}_3)\right]\bar{r}_3} \tag{14}$$

It is obvious that the disengagement will occur if $\theta_0>\theta_c$. Therefore, the relationship between the applied torque $\overline{M}_{1,QZS}$ and the torsional angle θ_1 from the rest position can be given by

$$\overline{M}_{1,QZS}=\begin{cases}\theta_1-\dfrac{1}{\bar{r}_3(1+\bar{r}_3)\bar{\delta}}\dfrac{\left[\bar{\delta}-(1+\bar{r}_3)+\bar{z}_4\right]\bar{r}_3\bar{z}_4\ \sin(\theta_1-\theta_0)}{\bar{z}_4-\bar{r}_3\ \cos(\theta_1-\theta_0)} & |\theta_1-\theta_0|\le\theta_c\\ \theta_1 & |\theta_1-\theta_0|>\theta_c\end{cases} \tag{15}$$

where

$$\bar{z}_4=\bar{r}_3\ \cos(\theta_1-\theta_0)+\sqrt{1-\bar{r}_3^2\sin^2(\theta_1-\theta_0)} \tag{16}$$

For the QZS isolator, the non-dimensional stiffness against the torsion angle are depicted in Fig. 3 when $\bar{r}_3=2$, which implies that the stiffness curves are notably affected by the initial compression δ. There exists a critical value of $\bar{\delta}$ that makes the range of torsion angle widest for small positive stiffness. As $\bar{\delta}$ increases to the critical value, the low stiffness range increases, and hence the value of 1.4 will be used in the following analysis.

When $\bar{r}_3=2$ and $\bar{\delta}=1.4$, the critical angle θ_c of disengagement and the static angle θ_0 are found to be 0.4214 and 0.5181, respectively. As mentioned before, the disengagement between the cam and the roller will occur in the case of $\theta_0>\theta_c$. Therefore, the relationship between the applied torque $\overline{M}_{1,QZS}$ and the torsional angle θ_1 from the rest position can be piecewise expressed by Eq. (15), which is depicted in Fig. 4. It shows two discontinuous points at $\theta_1=\theta_0-\theta_c$ and $\theta_1=\theta_0+\theta_c$, namely $\theta=-\theta_c$ and $\theta=\theta_c$, due to the disengagement. Furthermore, in the range of $\theta_0-\theta_c\le\theta_1\le\theta_0+\theta_c$, the cam keeps contact with the roller and the negative stiffness mechanism is active. Therefore, the stiffness in this range is lower than that in the ranges of $0\le\theta_1<\theta_0-\theta_c$ and $\theta_0+\theta_c<\theta_1\le2\theta_0$, in which the negative stiffness mechanism does not perform.

However, we only consider small torsional oscillations about the static equilibrium position, i. e. $|\theta|=|\theta_1-\theta_0|\le\theta_c$. Additionally, in the dynamic analysis, the static torque M_0 can be eliminated in the equation of motion. Thus, the relationship between the incremental torque $\overline{M}_{QZS}$ and the torsional angle θ from the static equilibrium position is depicted in the range $|\theta|\le\theta_c$, as shown in Fig. 5. It shows the typical quasi-zero stiffness characteristic around the equilibrium position. At the equilibrium position, the QZS isolator can hold a large static torque $\overline{M}_{1,QZS}=\overline{M}_0$, as shown in Fig. 4, similar to supporting a large mass for translational QZS isolators. When the shaft rotationally oscillates around the equilibrium position caused by the variation of excitation torque, the dynamic stiffness of the torsion QZS isolator is very small, and tends to zero at the equilibrium position.

In order to simplify the subsequent dynamic analysis, the relationship between torque and torsion angle is approximated by a polynomial using a Taylor series expansion up to the order of 7 expanded about the equilibrium position $\theta=0$, defined

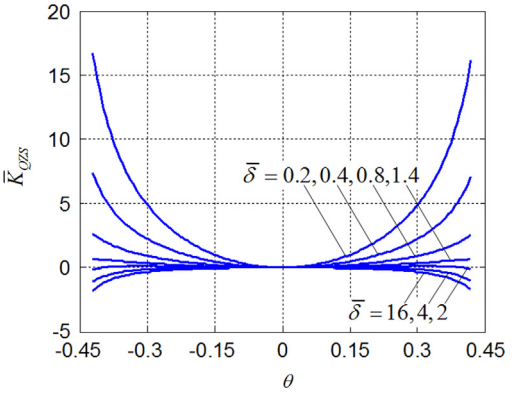

Fig. 3. Non-dimensional stiffness of the QZS isolator when $\bar{r}_3=2$.

Please cite this article as: J. Zhou, et al., A torsion quasi-zero stiffness vibration isolator, *Journal of Sound and Vibration* (2014), http://dx.doi.org/10.1016/j.jsv.2014.10.027

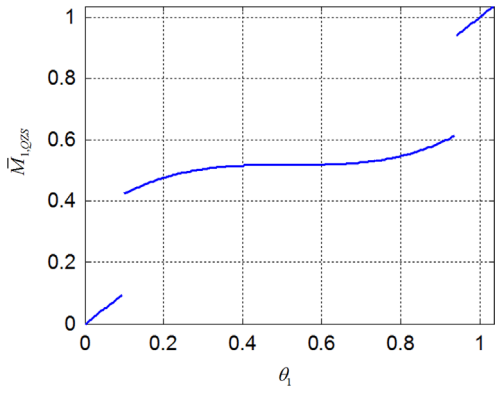

Fig. 4. Non-dimensional relationship between the applied torque $\overline{M}_{1,\mathrm{QZS}}$ and the torsion angle θ_1 from the rest position when $\bar{r}_3=2$, $\bar{\delta}=1.4$.

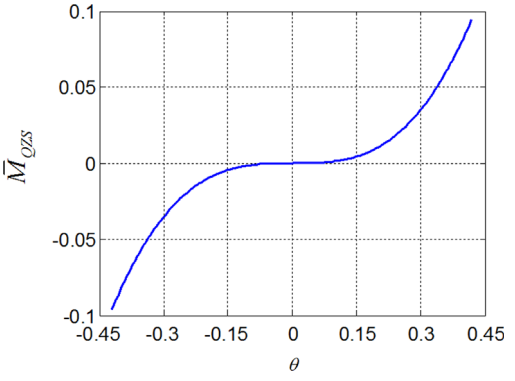

Fig. 5. Non-dimensional torque–torsion angle characteristic of the QZS isolator when $\bar{r}_3=2$, $\bar{\delta}=1.4$.

by

$$\overline{M}^{a}_{\mathrm{QZS}}=\overline{M}_{\mathrm{QZS}}(0)+\sum_{n=1}^{7}\frac{\overline{M}^{(n)}_{\mathrm{QZS}}(0)}{n!}\theta^{n} \tag{17}$$

where

$$\begin{gathered}\overline{M}_{\mathrm{QZS}}(0)=0,\ \ \overline{M}^{(1)}_{\mathrm{QZS}}(0)=0,\ \ \overline{M}^{(2)}_{\mathrm{QZS}}(0)=0,\ \ \overline{M}^{(4)}_{\mathrm{QZS}}(0)=0,\ \ \overline{M}^{(6)}_{\mathrm{QZS}}(0)=0\\ \overline{M}^{(3)}_{\mathrm{QZS}}(0)=3\left(\frac{1}{\bar{\delta}}-1\right)\bar{r}_3^2+3\left(\frac{1}{\bar{\delta}}+1\right)\bar{r}_3+1\\ \overline{M}^{(5)}_{\mathrm{QZS}}(0)=45\left(\frac{1}{\bar{\delta}}-1\right)\bar{r}_3^4+45\bar{r}_3^3-15\left(\frac{4}{\bar{\delta}}-1\right)\bar{r}_3^2-15\left(\frac{1}{\bar{\delta}}+1\right)\bar{r}_3-1\\ \overline{M}^{(7)}_{\mathrm{QZS}}(0)=1575\left(\frac{1}{\bar{\delta}}-1\right)\bar{r}_3^6-315\left(\frac{1}{\bar{\delta}}-5\right)\bar{r}_3^5-315\left(\frac{7}{\bar{\delta}}-3\right)\bar{r}_3^4\\ +315\left(\frac{1}{\bar{\delta}}-3\right)\bar{r}_3^3+63\left(\frac{11}{\bar{\delta}}-1\right)\bar{r}_3^2+63\left(\frac{1}{\bar{\delta}}+1\right)\bar{r}_3+1\end{gathered} \tag{18}$$

Let $\gamma_1=\overline{M}^{(3)}_{\mathrm{QZS}}(0)/3!$, $\gamma_2=\overline{M}^{(5)}_{\mathrm{QZS}}(0)/5!$ and $\gamma_3=\overline{M}^{(7)}_{\mathrm{QZS}}(0)/7!$, the approximate torque–torsion angle relationship can be rewritten as

$$\overline{M}^{a}_{\mathrm{QZS}}=\gamma_1\theta^3+\gamma_2\theta^5+\gamma_3\theta^7 \tag{19}$$

The exact solution of the QZS stiffness in the range $[-\theta_c,\ \theta_c]$ is compared with the approximate one as shown in Fig. 6a when $\bar{r}_3=2$ and $\bar{\delta}=1.4$, and Fig. 6b shows an excellent agreement with less than 1 percent error when the torsion angle is less than 0.3 rad (70 percent of the critical angle θ_c). Within the range of engagement of a cylindrical cam and roller pair, the maximum error is less than 9 percent. For another cases, such as $\bar{r}_3=2$, $\bar{\delta}=0.8$, and $\bar{r}_3=5$, $\bar{\delta}=1.1$, the errors are shown in Fig. 6c and d, respectively. It can be seen that in most of the range of angle the error is less than 5 percent, specifically about 82 percent and 86 percent of the critical angle θ_c for the two cases, respectively. It is significant that for small oscillations (about 35 percent of the critical angle θ_c for the three cases), the approximate expression using the polynomial form accurately matches the torque–torsion relationship.

Please cite this article as: J. Zhou, et al., A torsion quasi-zero stiffness vibration isolator, *Journal of Sound and Vibration* (2014), http://dx.doi.org/10.1016/j.jsv.2014.10.027

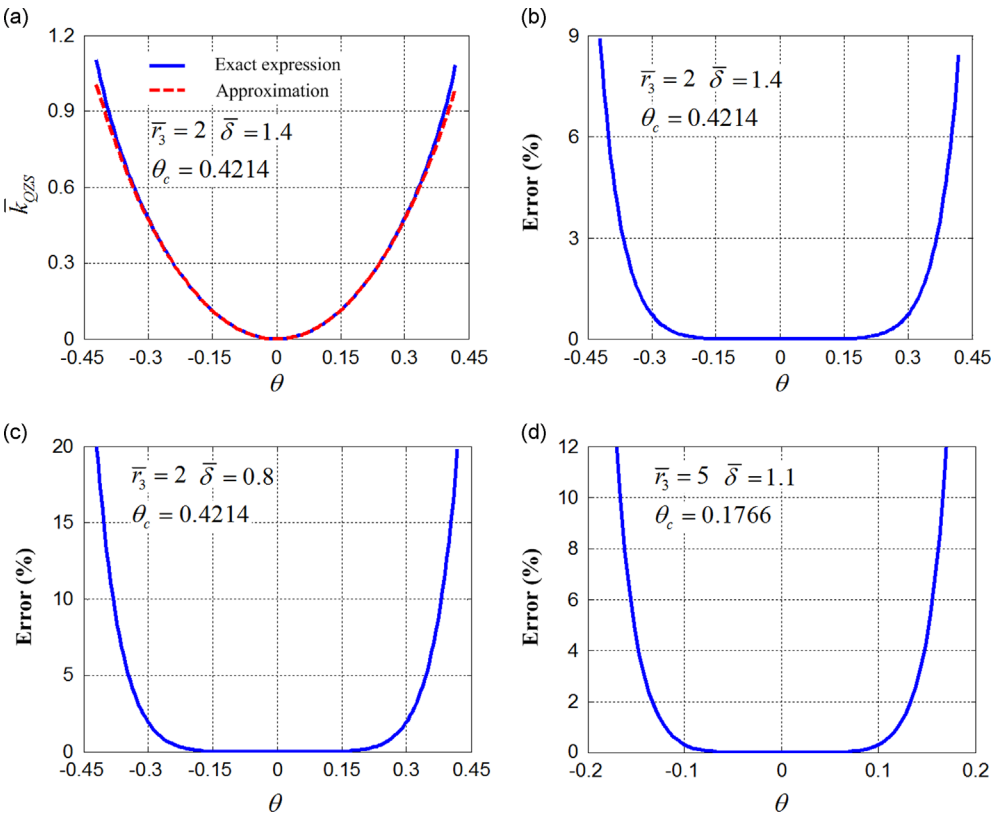

Fig. 6. (a) The exact expression of the QZS stiffness compared with the approximate one, and (b) error between the exact and approximate expressions for $\bar{r}_3 = 2$, $\bar{\delta} = 1.4$; (c) error for $\bar{r}_3 = 2$, $\bar{\delta} = 0.8$, and (d) error for $\bar{r}_3 = 5$, $\bar{\delta} = 1.1$.

3. Dynamic analysis

The QZS isolator is proposed in this paper to act as a shaft coupling with a characteristic of high-static–low-dynamic stiffness, and hence to isolate the low-frequency oscillatory torque being transmitted and suppress torsional vibrations. Therefore, potential applications in automotive transmission systems and propeller shat systems are expected.

Consider a power transmission from a motor to rotor though the shafts and the QZS isolator, as shown in Fig. 7. The motor on the left shaft outputs a designed torque M_0 in addition to a oscillatory torque $M_e \cos \omega t$, where ω is the excitation frequency and the designed torque M_0 is much larger than the excitation amplitude M_e. The QZS torsion vibration isolator plays a role to prevent the oscillatory torque being transmitted to the right hand shaft.

With the inclusion of a typical linear viscous damping term to account for dissipative terms, the equation of motion can be given by

$$I\ddot{\theta} + c\dot{\theta} + M_{QZS}(\theta) = M_e \cos \omega t \tag{20}$$

where I is the lumped inertia of the system, c is the damping coefficient, M_e is the amplitude of the oscillatory torque, and ω is the vibratory frequency. Using the following notations:

$$\omega_0 = \sqrt{\frac{k_\theta}{I}}, \quad \zeta = \frac{c}{2\sqrt{k_\theta I}}, \quad \overline{M}_e = \frac{M_e}{k_\theta \bullet 1}, \quad \Omega = \frac{\omega}{\omega_0}, \quad \tau = \omega_0 t \tag{21}$$

Eq. (20) can be rewritten as the non-dimensional form

$$\theta'' + 2\zeta\theta' + \overline{M}_{QZS}(\theta) = \overline{M}_e \cos \Omega\tau \tag{22}$$

where the prime $(\bullet)'$ represents differentiation with respect to τ. An analytical solution of Eq. (16) can be found by finding the first approximation of the primary resonance derived using the Harmonic Balance method. To simplify the subsequent algebraic work, we introduce a phase between torque and torsion in the force term, and Eq. (22) can be rewritten as

$$\theta'' + 2\zeta\theta' + \overline{M}_{QZS}(\theta) = \overline{M}_e \cos(\Omega\tau + \phi) \tag{23}$$

We assume the response solution to be

$$\theta = \Theta \cos \Omega\tau \tag{24}$$

Please cite this article as: J. Zhou, et al., A torsion quasi-zero stiffness vibration isolator, *Journal of Sound and Vibration* (2014), http://dx.doi.org/10.1016/j.jsv.2014.10.027

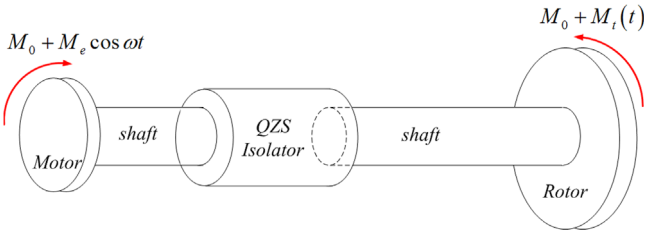

Fig. 7. Schematic diagram of the shaft system under vibratory torque.

Then using the approximate expression of restoring torque Eq. (19) and substituting Eq. (24) into Eq. (23) result in

$$\begin{aligned} &-\Theta\Omega^2 \cos \Omega\tau - 2\zeta\Omega\Theta \sin \Omega\tau + \frac{1}{4}\gamma_1\Theta^3(\cos 3\Omega\tau + 3\cos \Omega\tau) \\ &+\frac{1}{16}\gamma_2\Theta^5(\cos 5\Omega\tau + 5\cos 3\Omega\tau + 10\cos \Omega\tau) \\ &+\frac{1}{64}\gamma_3\Theta^7(\cos 7\Omega\tau + 7\cos 5\Omega\tau + 21\cos 3\Omega\tau + 35\cos \Omega\tau) \\ &= \overline{M}_e \cos \phi \cos \Omega\tau - \overline{M}_e \sin \phi \sin \Omega\tau \end{aligned} \tag{25}$$

Ignoring the high order harmonic terms, equating coefficients of $\cos \Omega\tau$ and $\sin \Omega\tau$, and then squaring and summing these results, the torsion amplitude –frequency relationship can be derived as

$$\left(-\Omega^2\Theta + \frac{3}{4}\gamma_1\Theta^3 + \frac{5}{8}\gamma_2\Theta^5 + \frac{35}{64}\gamma_3\Theta^7\right)^2 + (2\zeta\Omega\Theta)^2 = \overline{M}_e^2 \tag{26}$$

Solving the above quadratic equation for Ω^2 gives

$$\Omega_{1,2} = \sqrt{\frac{H}{\Theta} - 2\zeta^2 \pm \frac{1}{\Theta}\sqrt{4\zeta^4\Theta^2 - 4\zeta^2 H\Theta + \overline{M}_e^2}} \tag{27}$$

where $H = (3/4)\gamma_1\Theta^3 + (5/8)\gamma_2\Theta^5 + (35/64)\gamma_3\Theta^7$. The maximum torsion amplitude $\Theta_{\max}$ is when $\Omega_1 = \Omega_2$, i.e.

$$4\zeta^4\Theta^2 - 4\zeta^2\left(\frac{3}{4}\gamma_1\Theta^4 + \frac{5}{8}\gamma_2\Theta^6 + \frac{35}{64}\gamma_3\Theta^8\right) + \overline{M}_e^2 = 0 \tag{28}$$

As we shall show later, this expression produces a typical folded, nonlinear resonance curve with a jump phenomenon as the frequency is swept forwards and backwards. The jump down frequency Ω_d can be obtained by substituting $\Theta_{\max}$ into Eq. (27). Generally, the vibration isolation is effective when the excitation frequency is larger than the jump down frequency for a nonlinear vibration isolation system [20].

The torque transmitted to the right shaft can be described by

$$\begin{aligned} \overline{M}_t(t) &= 2\zeta\theta' + \overline{M}_{QZS}(\theta) \\ &= -2\zeta\Omega\Theta \sin \Omega\tau + \gamma_1\Theta^3 \cos^3\Omega\tau + \gamma_2\Theta^5 \cos^5\Omega\tau + \gamma_3\Theta^7 \cos^7\Omega\tau \\ &\approx -2\zeta\Omega\Theta \sin \Omega\tau + H\cos \Omega\tau \\ &= \sqrt{(2\zeta\Omega\Theta)^2 + H^2}\cos(\Omega\tau + \varphi) \end{aligned} \tag{29}$$

where $\tan \varphi = 2\zeta\Omega\Theta/H$. According to the usual definition, the torque transmissibility is defined by

$$T = \frac{\sqrt{(2\zeta\Omega\Theta)^2 + H^2}}{\overline{M}_e} \tag{30}$$

4. Responses and isolation performance

In this section, the parametrical region of the cam keeping contact with the roller will be presented, and the first approximation of response will be obtained for the parameters selected from the *contact region*. Furthermore, the vibration isolation performance will be evaluated by torque transmissibility, and the influences of excitation amplitude and damping factor on the isolation performance will be also discussed.

4.1. The first approximation of response

As mentioned earlier, only the case of small oscillation amplitude is considered here. The maximum amplitude in the frequency domain is strongly dependent on the excitation amplitude and the level of damping. Therefore, first of all, it is necessary to

determine the parameter range, in which the maximum oscillation response amplitudes do not exceed the critical torsion θ_c in order for the pair of cam and roller to always remain in contact during vibration. The maximum oscillation amplitude obtained by solving Eq. (28) as a function of excitation amplitude and damping is depicted in Fig. 8a. The pink, level surface represents the critical torsion amplitude $\Theta = \theta_c$. The cam and roller disengage when the oscillation torsion amplitude exceeds the critical value θ_c corresponding to the parameter region where the curved surface of $\Theta_{\max}$ is above the flat surface. The intersection between the curved surface of $\Theta_{\max}$ and the flat surface of $\Theta = \theta_c$ projected on to the parametric space $(\zeta,\ \overline{M}_e)$ gives a boundary $(\zeta_c,\ \overline{M}_{e,\,c})$ that divides the parameter space into two regions, as shown in Fig. 8b. To make sure that the cylindrical cam remains in contact with the roller, the parameters should be selected from the *contact region*.

For parameters selected from the *contact region*, the torsion amplitude–frequency relationships are shown in Fig. 9, in which solid line denotes stable solutions and dash line unstable ones. It can be observed that the responses are sensitive to damping and the excitation amplitude. The resonance branch shortens as the damping increases or the excitation amplitude decreases. The jump phenomenon even disappears for the comparatively large damping and small excitation amplitude. Therefore, a suitable damping is needed to suppress the resonant response.

4.2. Torque transmissibility

Generally, the nonlinear QZS vibration isolation system is effective only for the case when excitation frequencies exceed the jump down frequency. For given parameters, the jump down frequencies, for the present torsional QZS system, can be obtained by solving Eq. (28) and then substituting the solution subsequently into Eq. (27). The variations of jump down frequencies as functions of the damping factor and excitation amplitude are depicted in Fig. 10. Note that the value of the expression in the radical sign of Eq. (27) will become negative as the damping increases, which indicates the disappearance of jumping phenomenon, with the critical damping factors are denoted by hollow cycles in Fig. 10. It can be seen that the

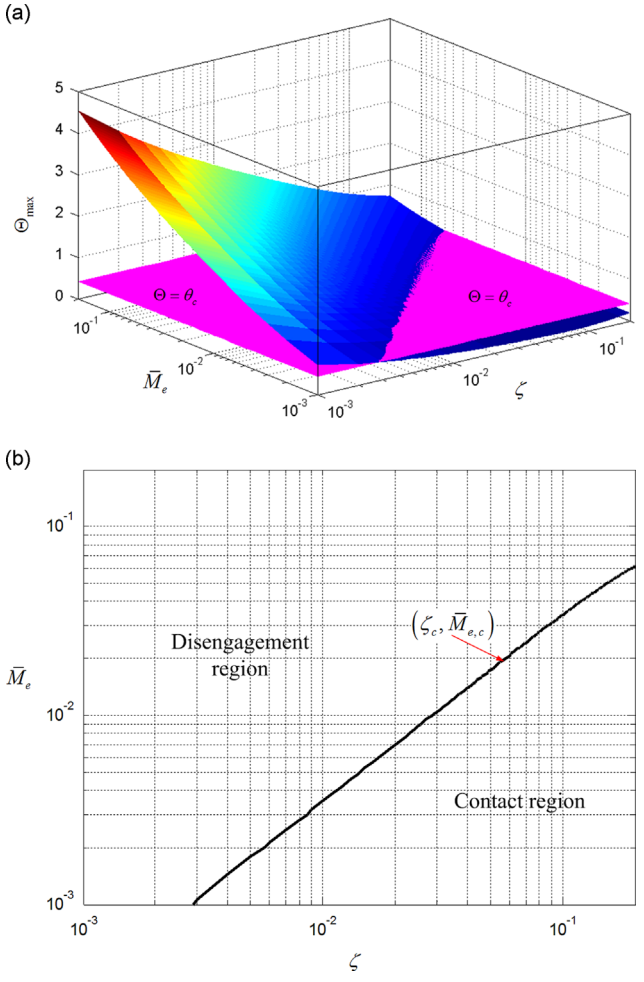

Fig. 8. Effects of the excitation amplitude and damping on the contact behavior between the cylindrical cam and roller. (a) Variations of the maximum torsion amplitude $\Theta_{\max}$ plotted against exciting amplitude and damping and the critical value of the torsion amplitude $\Theta = \theta_c$. (b) The parameter space $(\zeta,\ \overline{M}_e)$ divided into contact region and disengagement region by a boundary $(\zeta_c,\ \overline{M}_{e,c})$.

Please cite this article as: J. Zhou, et al., A torsion quasi-zero stiffness vibration isolator, *Journal of Sound and Vibration* (2014), http://dx.doi.org/10.1016/j.jsv.2014.10.027

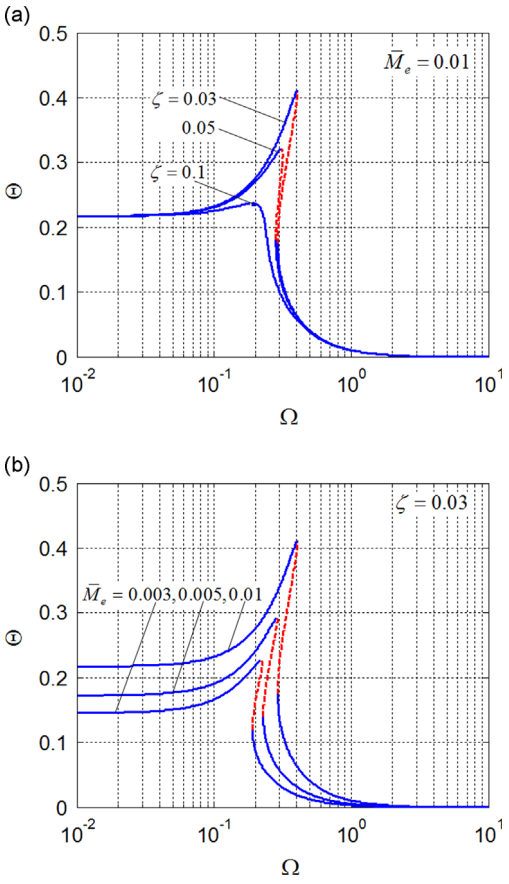

Fig. 9. Torsion amplitude–frequency curves influenced by (a) damping and (b) excitation amplitude. Solid and dash lines denote stable and unstable solutions, respectively.

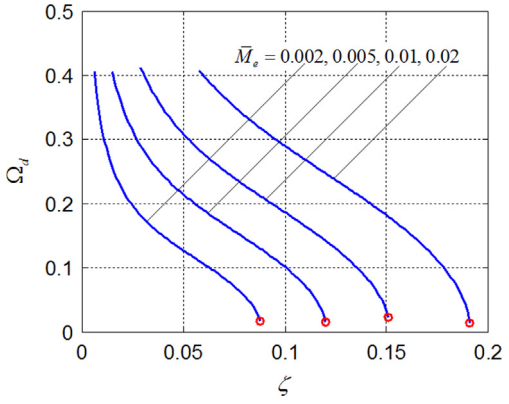

Fig. 10. Variations of jump down frequency of the QZS system plotted against damping and excitation amplitude. The hollow cycles donate the critical damping for disappearance of the jump phenomenon.

jump down frequency reduces with the increase in damping, but increases as the excitation amplitude increases. It is also observed that the jump-down frequencies for the parameters in the *contact region* are less than the natural frequencies of the corresponding linear system, i.e. $\Omega = 1$. The corresponding linear system is referred to a vibration isolation system only possessing the identical element of positive stiffness to that of the QZS system.

The torque transmissibility is evaluated by Eq. (30), and the peak (or maximum) transmissibility values are shown in Fig. 11. The peak transmissibility reduces with increase in damping and decrease in excitation amplitude. The peak transmissibility is also compared with that of the linear system shown as the dash dot line in Fig. 11. Under small excitations, such as $\bar{M}_e = 0.002,\ 0.005$, the peak transmissibility of the QZS system is less than that of the linear system. However, under

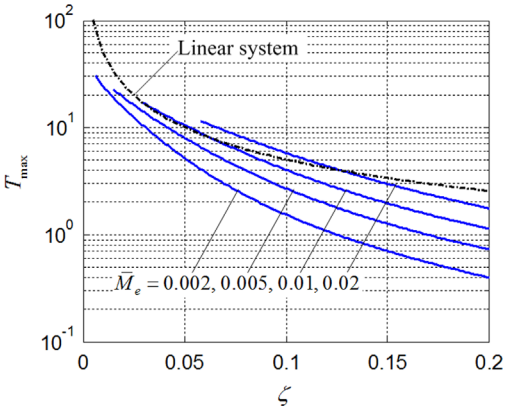

Fig. 11. Variations of maximum torque transmissibility of the QZS VIS against damping and exciting amplitude and compared with the linear system.

the large excitations, such as $\overline{M}_e = 0.02$, the peak transmissibility of the QZS system is larger than that of the linear system. Nevertheless, for most parameters in the *contact region*, the peak transmissibility of QZS system is smaller than that of the linear system.

Fig. 12 shows the oscillatory torque transmissibility of the QZS system with different parameters of damping and excitation amplitude in comparison with the linear system for a range of excitation frequencies. It can be observed that the effective frequency of vibration isolation of the QZS system is lower than that of the linear system, and the peak transmissibility of the QZS system is less than that of the linear system. Another important observation is that the transmissibility of the QZS system is lower than that of the linear system in the low-frequency range. Therefore, from the standpoint of low-frequency vibration isolation, the present torsion QZS vibration isolation system is superior to its corresponding linear system.

5. Study of mismatch of designed torque

It is known that translational QZS isolators can perform well under a designed loading weight. Similarly the torsional QZS isolator can most effectively perform torsional vibration attenuation under a design torque M_0 due to the fact that this torque positions the torsional QZS isolator in the equilibrium state which then produces the QZS property. In this regard, the torsional QZS isolator is only suitable for the application where the designed transmission torque is constant. Under this condition, with only small fluctuations of the transmission torque, the torsional QZS isolator can perform an excellent role of isolating torsional vibrations.

Consider a situation, when the actual transmission torque deviates from the designed torque M_0 by a percentage η, that is, the transmission torque changes form M_0 to $(1+\eta)M_0$. Given a torque fluctuation of $\overline{M}_e \cos \Omega\tau$ in this case, the equation of motion can be rewritten by

$$\theta'' + 2\zeta\theta' + \overline{M}_{QZS}(\theta) = \overline{M}_e \cos \Omega\tau + \eta\overline{M}_0 \tag{31}$$

where $\overline{M}_0 = M_0/(k_\theta \bullet 1)$. The increment of torque $\eta\overline{M}_0$ leads the torsional QZS isolator to have a new equilibrium position. This shift of equilibrium position undermines the critical condition in Eq. (8) for the zero stiffness characteristic at the designed equilibrium position, and degrades the isolation performance of the QZS isolator.

Fig. 13 shows the transmissibility of an excitation torque $\overline{M}_e \cos \Omega\tau$ when the incremental increase of torque $\eta\overline{M}_0$ at levels of η given by 0, 1, 5 and 10 percent, where $\overline{M}_e$ and ζ are set at 0.01 and 0.1, respectively. Note that the results in Fig.13 are achieved by solving Eq. (31) using Runge–Kutta method with swept sine input. It can be seen that the transmissibility curves increase as the torque difference increases. This clearly indicates that the isolation performance of the QZS isolator significantly deteriorates from that using the designed torque. Note that vibration isolation only occurs below the critical value of $T=0$. These worsening effects are mainly reflected in two issues. Firstly, the starting point for the available isolation frequency is increased as η increases, meaning that the advantage of vibration isolation of low-frequency bandwidth for the torsional QZS isolator is reduced. Secondly, values of the transmissibility in the frequency domain of the effective isolation all increase as the deviation of torque increases. It can be seen that the isolation performance is very sensitive to the change of torque. As mentioned before, the change of transmission torque results in a deviation of static equilibrium position from the original designed one, and leads to a significant increase of the stiffness of the system. Referring to Fig. 3, the system could become increasingly stiff as the deviation of the equilibrium positions grows, leading to an increasingly worse isolation performance.

In future work, a new type of torsional QZS isolator with a tunable mechanism will be developed to adaptively keep the position of the roller aiming at the cylindrical cam when the transmission torque changes. By so doing, the system's stiffness will retain the quasi-zero-stiffness property at various equilibrium positions and the excellent isolation performance could be achievable regardless of the variation of transmission torque.

Please cite this article as: J. Zhou, et al., A torsion quasi-zero stiffness vibration isolator, *Journal of Sound and Vibration* (2014), http://dx.doi.org/10.1016/j.jsv.2014.10.027

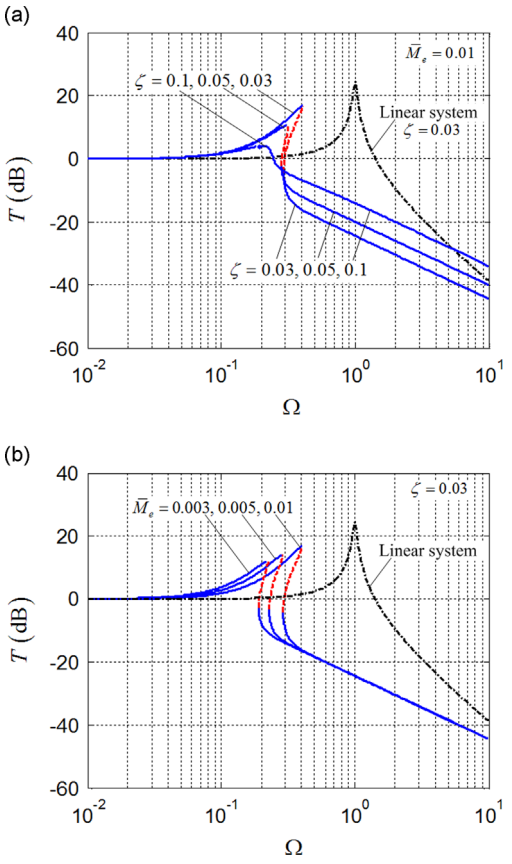

Fig. 12. Torque transmissibility of the QZS VIS influenced by (a) damping and (b) exciting amplitude, and compared with the linear system.

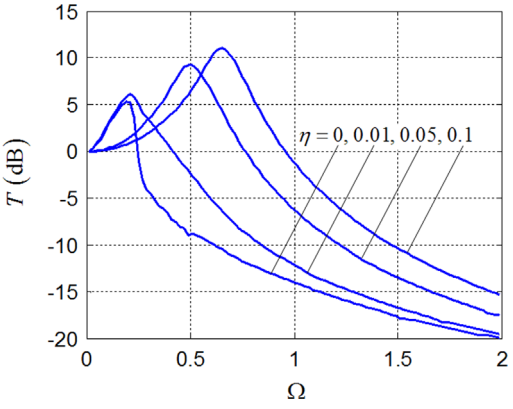

Fig. 13. Influence of variation of output torque on the torque transmissibility.

6. Conclusions

A novel quasi-zero stiffness isolator for torsional vibrations has been proposed. The static analysis was carried out to obtain the restoring torque. The system parameters were designed to meet the zero-stiffness-condition that makes the stiffness of the isolator zero at the equilibrium position. The equation of motion of the shaft system containing the QZS isolator has been established. Furthermore, the dynamic characteristics of the QZS torsional vibration isolation system were investigated using theoretical analysis.

The parameter regions of the excitation amplitude and the damping factor, in which the cylinder cams are ensured to remain in contact with a pair of the cylindrical cam and roller, were studied based on the fundamental solution of the equation of motion using the Harmonic Balance method. The isolation performance was evaluated by investigating the torque transmissibility. It was found that in the *contact regions*, the jump-down frequency of the QZS system is lower than

Please cite this article as: J. Zhou, et al., A torsion quasi-zero stiffness vibration isolator, *Journal of Sound and Vibration* (2014), http://dx.doi.org/10.1016/j.jsv.2014.10.027

the effective frequency of the linear counterpart, and the maximum transmissibility of the QZS system is also smaller than that of the linear system. In general, the torsional QZS isolator with the cam–roller–rubber mechanism can significantly improve torsional vibration attenuation.

This study also considers the issue of mismatching of the designed torque. The influence of the variation in the output torque on the torque transmissibility was discussed. It was found that the isolation performance of the QZS isolator is sensitive to a deviation of output torque change from the designed torque, and that this deviation can considerably reduce the isolation performance. Hence, the present design of the torsional QZS isolator should ideally be confined to applications where the designed transmission torque remains unchanged. Future work will focus on building a prototype of the torsional QZS isolator and carrying out experimental investigations to confirm its effectiveness.

Acknowledgment

This research work was supported by the National Natural Science Foundation of China (11102062), Specialized Research Fund for the Doctoral Program of Higher Education (20110161120040, 20130161110037), and Fundamental Research Funds for the Central Universities.

References

[1] A. Carrella, M.J. Brennan, T.P. Waters, Static analysis of a passive vibration isolator with quasi-zero-stiffness characteristic, *Journal of Sound and Vibration* 301 (3–5) (2007) 678–689.
[2] A. Carrella, M.J. Brennan, I. Kovacic, T.P. Waters, On the force transmissibility of a vibration isolator with quasi-zero-stiffness, *Journal of Sound and Vibration* 322 (4–5) (2009) 707–717.
[3] A. Carrella, M.J. Brennan, T.P. Waters, K. Shin, On the design of a high-static-low-dynamic stiffness isolator using linear mechanical springs and magnets, *Journal of Sound and Vibration* 315 (3) (2008) 712–720.
[4] I. Kovacic, M.J. Brennan, T.P. Waters, A study of a nonlinear vibration isolator with a quasi-zero stiffness characteristic, *Journal of Sound and Vibration* 315 (3) (2008) 700–711.
[5] D. Xu, Y. Zhang, J. Zhou, J. Lou, On the analytical and experimental assessment of performance of a quasi-zero-stiffness isolator, *Journal of Vibration and Control* (2013), http://dx.doi.org/10.1177/1077546313484049.
[6] C.C. Lan, S.A. Yang, Y.S. Wu, Design and experiment of a compact quasi-zero-stiffness isolator capable of a wide range of loads, *Journal of Sound and Vibration* 333 (20) (2014) 4843–4858.
[7] T.D. Le, K.K. Ahn, A vibration isolation system in low frequency excitation region using negative stiffness structure for vehicle seat, *Journal of Sound and Vibration* 330 (2011) 6311–6335.
[8] D. Platus, Negative-stiffness-mechanism vibration isolation systems, *Proceedings of the SPIE's International Symposium on Vibration control in Microelectronics, Optics and Metrology* (1991).
[9] J. Yang, Y.P. Xiong, J.T. Xing, Dynamics and power flow behaviour of a nonlinear vibration isolation system with a negative stiffness mechanism, *Journal of Sound and Vibration* 332 (1) (2013) 167–183.
[10] A. Carrella, M. Friswell, A passive vibration isolator incorporating a composite bistable plate, *Proceedings of the Sixth EUROMECH Nonlinear Dynamics Conference* (*ENOC 2008*), Saint Petersburg, Russia, 2008.
[11] A.D. Shaw, S.A. Neild, D.J. Wagg, P.M. Weaver, A. Carrella, A nonlinear spring mechanism incorporating a bistable composite plate for vibration isolation, *Journal of Sound and Vibration* 332 (24) (2013) 6265–6275.
[12] X. Sun, X. Jing, J. Xu, L. Cheng, Vibration isolation via a scissor-like structured platform, *Journal of Sound and Vibration* 333 (9) (2014) 2404–2420.
[13] W.S. Robertson, M.R.F. Kidner, B.S. Cazzolato, A.C. Zander, Theoretical design parameters for a quasi-zero stiffness magnetic spring for vibration isolation, *Journal of Sound and Vibration* 326 (1-2) (2009) 88–103.
[14] D. Xu, Q. Yu, J. Zhou, S.R. Bishop, Theoretical and experimental analyses of a nonlinear magnetic vibration isolator with quasi-zero-stiffness characteristic, *Journal of Sound and Vibration* 332 (14) (2013) 3377–3389.
[15] W. Wu, X. Chen, Y. Shan, Analysis and experiment of a vibration isolator using a novel magnetic spring with negative stiffness, *Journal of Sound and Vibration* 333 (13) (2014) 2958–2970.
[16] N. Zhou, K. Liu, A tunable high-static-low-dynamic stiffness vibration isolator, *Journal of Sound and Vibration* 329 (2010) 1254–1273.
[17] X. Sun, J. Xu, X. Jing, L. Cheng, Beneficial performance of a quasi-zero-stiffness vibration isolator with time-delayed active control, *International Journal of Mechanical Sciences* 82 (2014) 32–40.
[18] P. Alabuzhev, A. Gritchin, L. Kim, G. Migirenko, V. Chon, P. Stepanov, *Vibration protecting and measuring system with quasi-zero stiffness*, Taylor & Francis Group, New York, 1989.
[19] R.A. Ibrahim, Recent advances in nonlinear passive vibration isolators, *Journal of Sound and Vibration* 314 (3–5) (2008) 371–452.
[20] B. Ravindra, A.K. Mallik, Performance of non-linear vibration isolators under harmonic excitation, *Journal of Sound and Vibration* 170 (3) (1994) 325–337.

Please cite this article as: J. Zhou, et al., A torsion quasi-zero stiffness vibration isolator, *Journal of Sound and Vibration* (2014), http://dx.doi.org/10.1016/j.jsv.2014.10.027